

Origin of second harmonic generation in non-centrosymmetric crystal structures containing lone-pairs electrons

Fuming Li^{1,2}, Shilie Pan^{1,2,*}, and Zhihua Yang^{1,2†}

¹Research Center for Crystal Materials; CAS Key Laboratory of Functional Materials and Devices for Special Environmental Conditions; Xinjiang Key Laboratory of Functional Crystal Materials; Xinjiang Technical Institute of Physics and Chemistry, Chinese Academy of Sciences, Urumqi 830011, China and

²Center of Materials Science and Optoelectronics Engineering, University of Chinese Academy of Sciences, Beijing 100049, China

Material systems with lone-pair electrons have long been a treasure trove in the search for large second harmonic generation effects. Revealing the origin of second harmonic generation in non-linear optical materials can provide theoretical guidance for the design of new materials. In this work, the origin of second harmonic generation in non-centrosymmetric materials containing lone pair electrons is revealed by analyzing the orbital interactions on the sublattice. Stereochemically inactive Pb 6s orbitals with high symmetry in CsPbCO₃F contribute less to the second harmonic generation. In contrast, the contribution of stereochemically active Pb 6s orbital in PbB₅O₇F₃ and PbB₂O₃F₂ is more obvious. Significantly, the orbitals of the interaction between lead and oxygen make a very significant contribution because these orbitals are located at the band edge and in non-centrosymmetric sublattices.

PACS numbers: 61.66.FN, 61.50.Ah, 71.20.-b

I. INTRODUCTION

Nonlinear optical (NLO) effects play an important role in fundamental scientific research and the practical application of high-performance optoelectronic materials [1–6]. NLO materials exhibit an extraordinary ability to convert laser frequencies *via* second harmonic generation (SHG). The polarization dependence of SHG can provide rich information about the structural symmetry of the material and the microscopic arrangement of chemical bonds [7–11]. The atomic orbitals in materials form hybrid orbitals with diverse shapes and energies, which reflects the characteristics of chemical bonds and molecular geometry [12]. Generally, the chemical-bond-associated microstructures determine the physico-chemical properties of materials, which are inseparable from the covalent interaction (*e.g.*, B/P-O bonds) of microscopic groups or driven of electrostatic ionic systems (*e.g.*, M_xO_y polyhedron, M is for metal elements) [13, 14]. For example, depending on the asymmetric charge distribution of π orbital itself, the material may have a large SHG effect [15]. For materials with ns^2 lone-pair electron cations such as Pb²⁺, Bi³⁺ and I⁵⁺, the interaction of cation *s*-state and anion *p*-state orbitals can affect the strength of chemical bonds and deform the distortion of coordination geometry [16], which gives rise to some interesting and fascinating physical properties [17, 18]. For example, it plays an important role in both the exciton relaxation and dissociation of low-dimensional halide perovskites [19]. Lone pair also can increased phonon dissonance, resulting in low lattice thermal conductivity [20]. In NLO materials, lone-pair electron cations may improve the microscopic second-order polarizability of ionic groups, thereby inducing greater NLO properties [21–23]. Reasonably as-

sembling polar units can be used to effectively design non-centrosymmetric materials with excellent SHG performance [24]. For example, the IO₃ group belongs to the lower symmetry C_{3v} group compared with BO₃ (D_{3h}) own to the lone-pair electrons on the iodine atom and has a large microscopic second-order polarizability [25]. The SHG effect can be enhanced by condensing IO₃ in a parallel arrangement in each unit cell, such as α -LiIO₃ crystal [26]. Therefore, material systems with lone-pair electrons have long been a treasure trove in the search for large SHG effects.

Lone-pair electrons can exhibit varying degrees of stereochemical activity or even inactivity, which is governed by crystal symmetry and orbital energy differences [16]. The asymmetric distribution of electron clouds at the band edge dictates that the stereochemically active lone-pair electrons can induce excellent optical properties of materials. For example, SbB₃O₆ contains the stereochemically active lone-pair Sb³⁺ cation, which gives it the highest birefringence (0.290 at 546 nm) among borate materials, and also exhibits a strong SHG effect of $3.5 \times \text{KH}_2\text{PO}_4$ (KDP) [27]. On the other hand, significant SHG effects can also be enhanced by *p*- π interactions of cations and π -conjugated groups in materials containing stereochemical inactivity, *e.g.*, CsPbCO₃F [28]. Understanding the structure-property relationships of these materials is crucial for elucidating the effect of lone-pair electrons on SHG. The wave function analysis under local representation in periodic lattice potential field provides an effective method to study the factors affecting the optical properties of materials [29]. Currently, the influence of lone-pair electrons with different levels of stereochemical activity to the SHG effect has not been directly studied at the orbital level. Specifi-

cally, quantitative studies are still needed regarding the direct contribution of cations with ns^2 lone-pair electrons to the SHG coefficient and the influence of the orbitals through which these cations interact with surrounding anions. In this work, we investigated the origin of SHG in materials containing different stereochemically active lone-pair electrons.

II. COMPUTATIONAL ANALYSIS METHOD

All first-principles simulations were performed using Vienna *ab initio* simulation package (VASP) [30]. The exchange-correlation potential and ion-electron interaction were described by the Perdew-Burke-Ernzerhof (PBE) functional and projector-augmented wave (PAW) methods, respectively. The valence electron configurations were treated as follows: Cs- s,p,d , Pb- s,p,d , Sn- s,p,d , B- s,p , C- s,p , O- s,p and F- s,p . First, the Broyden-Fletcher-Goldfarb-Shannon (BFGS) algorithm is used to optimize the atomic position and lattice parameters [31, 32], and the atoms are allowed to relax until the force applied to the atom is less than 0.02 eV/Å. An energy cutoff of 400 eV and specific Monkhorst-Pack k -point meshes of $7 \times 7 \times 7$ for CsPbCO₃F, $3 \times 4 \times 4$ for PbB₅O₇F₃, and $9 \times 9 \times 7$ for PbB₂O₃F₂ were used. Second, during the static self-consistent-field calculation, the plane-wave cutoff energy of 600 eV and the threshold of 10^{-7} eV, where the k -point meshes is consistent with the above. Third, the Wannier orbitals are constructed through a post processing procedure using the output of VASP calculation, and the corresponding orbitals type by the projection of all valence states in the unit cell were generated using WANNIER90 [33–35]. And the plane-wave cutoff energy of 800 eV, threshold of 10^{-10} eV and dense Monkhorst Pack k -point mesh spanning remains the same. Fourth, the optical properties of all compounds and the SHG contribution of each Wannier orbital were calculated. For the optical property calculations, the plane-wave cutoff energy of 800 eV, energy threshold of 10^{-10} eV, and a Monkhorst-Pack k -point mesh with a density twice that used in the self-consistent-field calculation were applied to ensure higher precision.

The i, j, k are Cartesian components, v and v' denote valence bands, c and c' denote conduction bands, and $P(ijk)$ denotes full permutation and explicitly shows the Kleinman symmetry, which ensures the frequency-

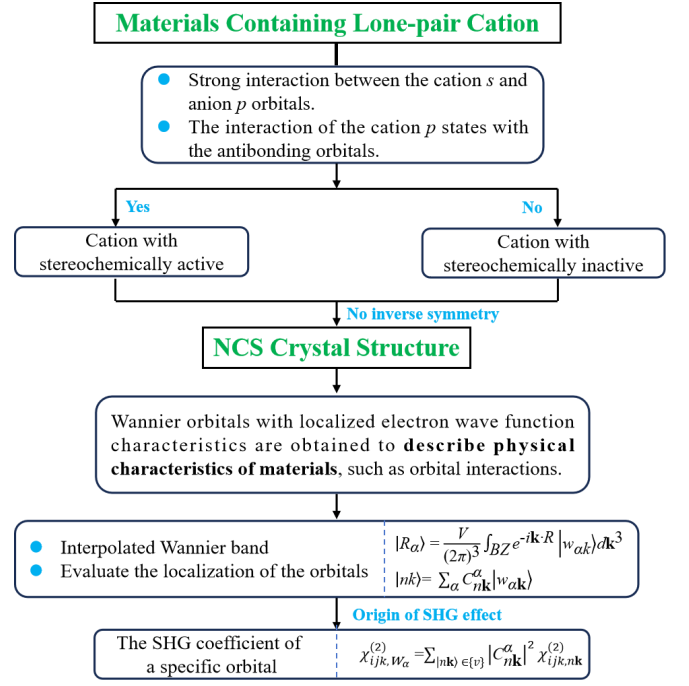


FIG. 1: (Color online) The decision tree to analyze the origin of SHG coefficient of materials.

The length gauge formalism method, originally developed by Aversa and Sipe [36], has proven effective in avoiding unphysical divergences that may arise in NLO calculations. Rashkeev et al.[37] rearrange their formula, and its static frequency doubling coefficient calculation formula can be further simplified, the frequency dependent form derived from the length gauge method can be simplified to the form derived from the dynamic gauge method [38]. At zero frequency, the SHG coefficients d_{im} can be derived by transforming from the second-order susceptibility tensor $\chi_{ijk}^{(2)}$, where the relationship is given as $d_{im} = \frac{1}{2}\chi_{ijk}^{(2)}$. Specifically, they are calculated using the following expression:

$$\chi_{ijk}^{(2)} = \chi_{ijk}^{(2)}(VE) + \chi_{ijk}^{(2)}(VH), \quad (1)$$

$$\chi_{ijk}^{(2)}(VE) = \frac{e^3}{2\hbar^2 m^3} \sum_{vcc'} \int \frac{d\mathbf{k}^3}{4\pi^3} P(ijk) \text{Im}[p_{vc}^i p_{c'c'}^j p_{c'v}^k] \left(\frac{1}{\omega_{cv}^3 \omega_{v'c'}^2} + \frac{2}{\omega_{vc}^4 \omega_{c'v}} \right), \quad (2)$$

$$\chi_{ijk}^{(2)}(VH) = \frac{e^3}{2\hbar^2 m^3} \sum_{vv'c} \int \frac{d\mathbf{k}^3}{4\pi^3} P(ijk) \text{Im}[p_{v'v}^i p_{v'c}^j p_{cv}^k] \left(\frac{1}{\omega_{cv}^3 \omega_{v'c}^2} + \frac{2}{\omega_{vc}^4 \omega_{c'v'}} \right), \quad (3)$$

independent nature of the nonlinear susceptibility tensor. In addition, the contribution of the two-band transition process has been strictly proved to be zero through rigorous theoretical analysis.

Figure 1 presents a decision tree framework for analyzing the origin of SHG coefficients in crystalline materials. For specific materials, the analysis first evaluates the stereochemical activity of lone-pair electrons by examining two key factors: the coordination symmetry around the cation and the orbital energy alignment between cation and anion orbitals. Then, by combining information about the crystal symmetry (centrosymmetric or non-centrosymmetric) with the degree of stereochemical activity of lone pairs, their effects on the material microstructure and SHG response can be further analyzed.

Using a unitary transformation, a set of Wannier functions (WFs) $\mathbf{R}(r)$, labeled by the Bravais lattice vector \mathbf{R} , can be constructed from the Bloch eigenstates $|n\mathbf{k}\rangle$ of band n . This transformation preserves all the physical information while providing a more intuitive real-space picture of the electronic structure. The Bravais lattice vector \mathbf{R} helps identify the spatial location of these localized functions within the crystal structure. To quantitatively evaluate the contribution of Wannier orbitals to the SHG response, a projection procedure is implemented. All valence states $|n\mathbf{k}\rangle \in \{v\}$ (where $\{v\}$ represents the set of all valence bands) are projected onto atomlike Wannier orbitals $|w_\alpha\rangle$. Through this projection, we obtain the coefficients C_{nk}^α , which quantify how much each atomlike Wannier orbital contributes to each valence state. The square of the magnitude of these projection coefficients, $|C_{nk}^\alpha|^2$, represents the weight or contribution of the Wannier orbital w_α to the n -th valence band-decomposition [39]. This decomposition allows us to directly evaluate the orbital-resolved contributions to the SHG response, providing detailed insights into the microscopic origin of NLO properties [40].

III. RESULTS AND DISCUSSION

To illustrate the types of stereochemical activity and inactivity lone-pair electron at different sublattice and

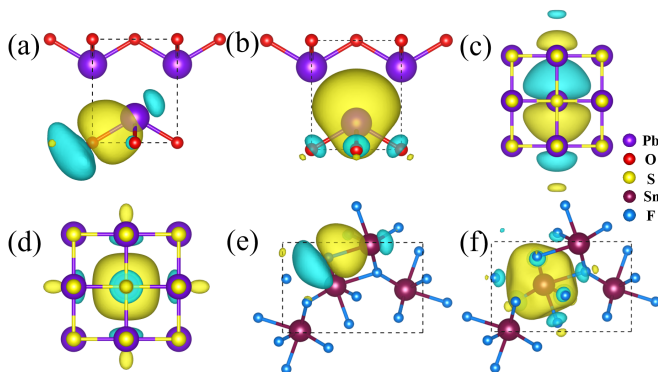


FIG. 2: (Color online) The Pb-O ionic orbital (a) and Pb 6s orbital (b) in litharge PbO. The Pb-S ionic orbital (c) and Pb 6s orbital (inactivity) (d) in rocksalt PbS. The Sn-F ionic orbital (e) and Sn 5s orbital (f) in β -SnF₂.

their effects on electronic structural distortion, we first describe the orbital interactions in the valence bands of litharge PbO and rocksalt PbS. The interpolated bands of maximally projected WF's are shown in dotted lines in Figs. S1a-S1b, which matches the original band structure (solid line), indicating that well localized of the Wannier orbital. Here, the Wannier orbital is a linear combination of all relevant atomic orbitals in energy space. Interactions between these atomic orbitals cause the shape of WF's to deviate from the standard atomic orbitals. Figures 2(a)–2(d) show the Wannier orbital of lead and the oxygen/sulfur-centered for PbO and PbS. The features of oxygen orbitals expand in the direction of lead and have covalent characteristics with lead consist of Pb 6s/6p and O 2p [see Fig. 2(a)]. The differences of Pb 6s orbitals can be observed, which shows the activity and inactivity of lone-pair electrons in PbO and PbS, respectively. In PbO, a highly asymmetric lobe is away from lead, which is determined by the anti-bonding (Pb 6s + O 2p)* and Pb 6p. In contrast, lead in PbS is constrained by the symmetry of surrounding sulfur atoms, the Pb 6s orbitals exhibit a completely symmetrical shape and will not exhibit stereochemical activity. The litharge PbO and rocksalt PbS structure locate in a centrosymmetric space group, so all orbitals forming centrosymmetric sublattices and do not contribute to SHG. In contrast, β -SnF₂ is located in a chiral $P4_12_12_1$ space group, and similar methods were used to analyze orbital interactions (Fig. 2(e)–2(f)). The Sn 5s orbital of β -SnF₂ also exhibits an asymmetric electronic distribution, and the symmetry analysis shows that the Sn 5s orbital is located in a non-centrosymmetric sublattice, which dominates the contribution to the SHG.

To identify the origin of SHG in materials with different stereochemical activity materials at the orbital level, we analyzed the SHG properties of CsPbCO₃F, PbB₅O₇F₃ and PbB₂O₃F₂ by examining their lattice symmetries and electronic structures. Here, we first divided the sublattices of the crystal structure of these materials, which can be decomposed into different chemical environment sublattices containing cations, carbon,

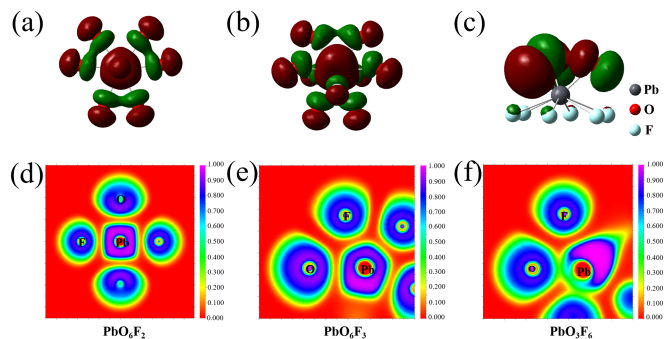


FIG. 3: (Color online) The highest occupied molecular orbital (HOMO) (a-c) and ELF diagram (d-f) of PbO₆F₂, PbO₆F₃ and PbO₃F₆ in CsPbCO₃F, PbB₅O₇F₃ and PbB₂O₃F₂.

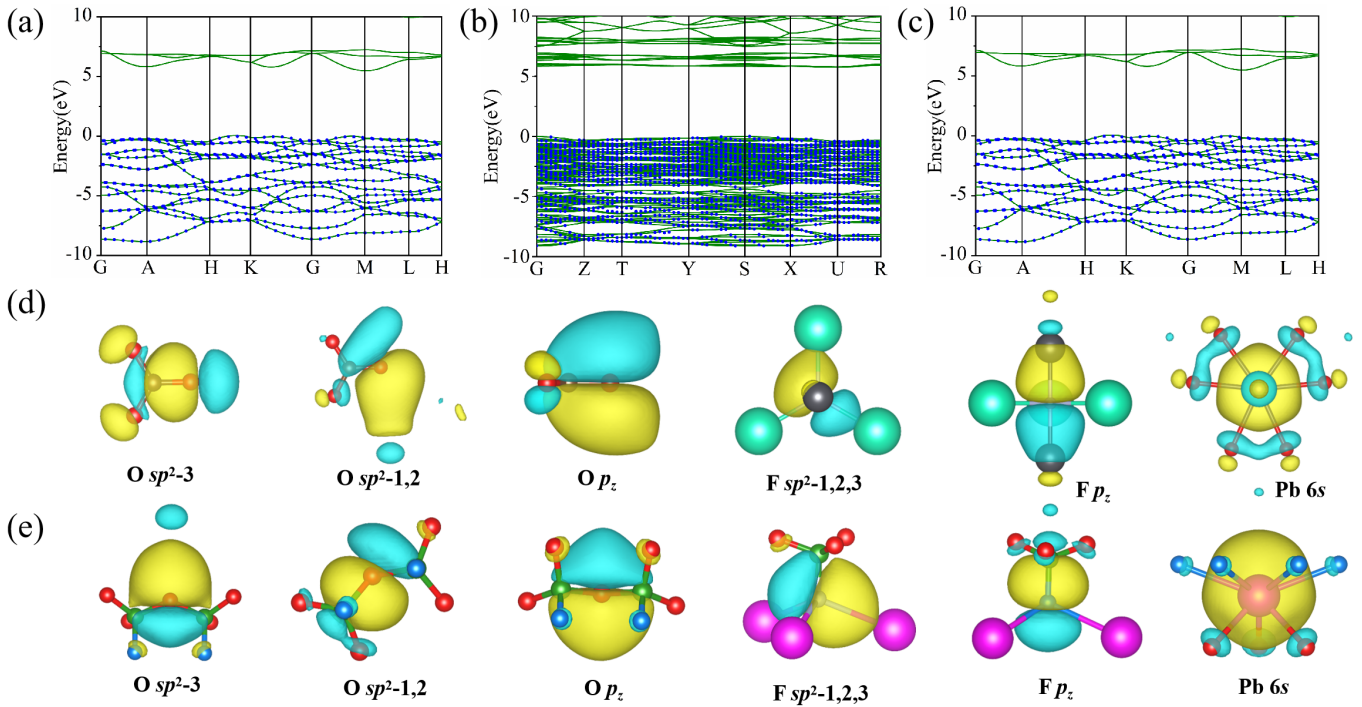


FIG. 4: (Color online) The band structure (solid lines: DFT bands; dots: Wannier-interpolated bands) of CsPbCO₃F (a), PbB₅O₇F₃ (b) and PbB₂O₃F₂ (c). Wannier orbitals of oxygen, fluorine and lead in CsPbCO₃F (d): from left to right are: the orbital of σ bonds between carbon and oxygen (O sp^2-3); the orbital of ionic interaction between oxygen and lead (O $sp^2-1,2$); nonbonding orbital of oxygen (O p_z); the orbital of ionic interaction between fluorine and cesium (F $sp^2-1,2,3$); the orbital of ionic interaction between fluorine and lead (F p_z); and Pb 6s orbital. Wannier orbitals of oxygen, fluorine and lead in PbB₂O₃F₂ (e): the orbital of ionic interaction between oxygen and lead (O sp^2-3); the orbital of σ bonds between boron and oxygen (O $sp^2-1,2$); nonbonding orbital of oxygen (O p_z); the orbital of ionic interaction between fluorine and lead (F $sp^2-1,2,3$); the orbital of σ bonds between fluorine and boron (p_z); and Pb 6s orbital.

boron, oxygen and fluorine. Analysis of the sublattice symmetries revealed that the carbon and oxygen sublattices in CsPbCO₃F, as well as the boron and oxygen/fluorine sublattices in PbB₅O₇F₃ and PbB₂O₃F₂, lack a symmetric inversion center at the unit cell, so they are in the non-centrosymmetric sublattices. In CsPbCO₃F, lead is constrained by the symmetry of surrounding oxygen and fluorine atoms, and their lone-pair electron show stereochemical inactivity. The F p_z orbital connected to Pb is located on the centrosymmetric sublattices ($P6/mmm$), and the interaction orbital between fluorine and cesium located in the non-centrosymmetric sublattices ($P\bar{6}m2$), so their possible SHG contributions may be different. The covalent interaction of the Pb 6s and O 2p orbitals makes lead-oxygen located in the non-centrosymmetric sublattice in PbB₅O₇F₃ and PbB₂O₃F₂, and asymmetric lobe of Pb 6s requires O 2p to participate in the formation. We investigated the symmetry of the electronic structure of the [PbO_nF_m] polyhedral unit of the material at the molecular orbital level (Fig. 3). The electronic wave function analysis is based on multiwfn software [41]. Both the highest occupied molecular orbital (HOMO) and electron local function (ELF) diagrams confirmed that the lone pair

electron activity follows the order: PbO₃F₆ > PbO₆F₃ > PbO₆F₂, corresponding to PbB₂O₃F₂, PbB₅O₇F₃ and CsPbCO₃F respectively.

To quantitatively determine the orbital contributions to the SHG coefficient from specific sublattices, we employed the symmetry-adapted WFs method. In this approach, the local orbital directions are strictly defined according to both the sublattice symmetry and coordination environment (Fig. S2). The well consistency of the interpolation Wannier and DFT band structures are shown in Figures. 4(a)–4(c), indicating that the orbitals we defined are well localized. The calculated SHG coefficients for these materials were given in Table S2. By comparing the magnitude of experimental powder SHG effect, it is demonstrated that our calculation results are reliable. For CsPbCO₃F [see Fig. 4(e)], the SHG contribution of the Pb 6s orbitals was calculated and found to be insignificant (-2 %) to the SHG. In contrast, the asymmetry of the Pb 6s orbital in PbB₅O₇F₃ and PbB₂O₃F₂ [see Fig. 4(f)] indicates that lone-pair electron is stereochemical activity and contributes more to SHG (6 % and 10 %). It is worth noting that the interactions orbitals between lead and oxygen contribute significantly to the SHG, with 54, 29 and 34 % for CsPbCO₃F,

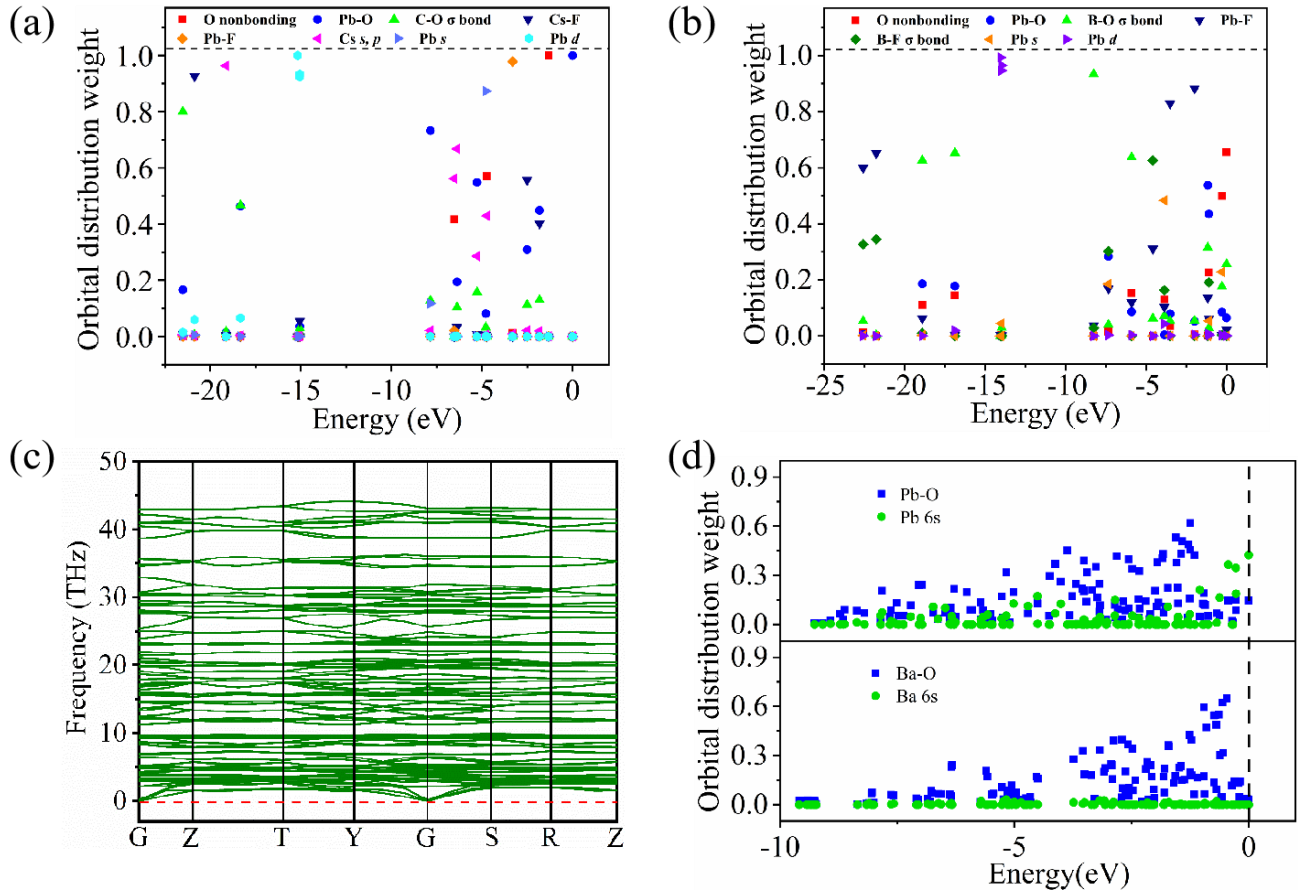


FIG. 5: (Color online) The orbital distribution weight at the energy level at Γ point of (a) CsPbCO₃F and (b) PbB₂O₃F₂. (c) Phonon spectrum curve of BaB₅O₇F₃ after lead replaced barium for PbB₅O₇F₃. (d) The orbital distribution weight of Pb/Ba-O, Pb 6s and Ba 6s for PbB₅O₇F₃ and BaB₅O₇F₃.

PbB₅O₇F₃ and PbB₂O₃F₂, respectively. This means that in CsPbCO₃F, p - π hybridization can show a strong SHG effects. In PbB₅O₇F₃ and PbB₂O₃F₂, the interaction between cation and anion groups makes an important contribution to the SHG effects, and the strong stereochemically active lead-oxygen orbitals of lone pair electrons may contribute more. On the other hand, the O nonbonding orbital also contribute significantly to the SHG, with 25, 56 and 17 % for CsPbCO₃F, PbB₅O₇F₃ and PbB₂O₃F₂, respectively. In comparison, C/B-O σ covalent bond contribute modestly. For fluorine-related orbitals, its contribution to the SHG is not negligible. Among them, the contributions of interactions orbitals between fluorine and lead/cesium in CsPbCO₃F are 3 and 29 %, respectively, which are consistent with the results of symmetry analysis. Among the atoms in non-centrosymmetric sublattice, the contribution to SHG was determined by their distribution in the energy space. Therefore, we need to analyze the SHG contribution of sublattice on orbitals in energy space.

To more clearly observe the distribution of the orbital in the energy space, the SHG coefficients calculated at Γ points is used as a reference for the clarity for CsPbCO₃F

and PbB₂O₃F₂. Figures. 5(a)–5(b) show the orbital distribution weight at the Γ point of CsPbCO₃F. The interaction orbital between lead and oxygen, and oxygen nonbonding orbital have a substantial weight at the band edges. Moreover, the ionic bonds between fluorine and cesium for CsPbCO₃F, and the Pb 6s orbital for PbB₂O₃F₂ also have a clear distribution at the band edges. These orbitals dominate the contribution of the SHG coefficient. The orbitals of σ bonds between C/B-O/F are mainly distributed in the deep-level regions, and contribute weakly to SHG. Here, we constructed the isomorphic BaB₅O₇F₃ by using barium instead of lead to change the distribution of the band-edge orbitals of PbB₅O₇F₃ to illustrate the role of stereochemically active lead in the SHG effects. The dynamics of BaB₅O₇F₃ are stable [see Fig. 5(c)] and its shortest phase-matched wavelengths (184 nm, Fig. S4) is blue-shifted compared to PbB₅O₇F₃ (240 nm). We analyzed the orbital distribution weights of Pb/Ba-O, Pb 6s and Ba 6s in the energy space [see Fig. 5(d)]. The barium instead of lead causes blue-shift of band gap, which will reduce SHG. In addition, the s orbital of the metal cation is far away from the band edge. Calculation results also

show that compared to $\text{PbB}_5\text{O}_7\text{F}_3$, the calculated SHG coefficient of $\text{BaB}_5\text{O}_7\text{F}_3$ are decreased sharply (decreased by 63 %). The Ba 6s orbitals are almost spherical compared to the asymmetric distribution of the Pb 6s orbitals in $\text{PbB}_5\text{O}_7\text{F}_3$, and contribute almost zero to the SHG. Therefore, lead plays an indispensable role in the origin of the SHG, which arises from orbitals of cation and anion group interactions on the non-centrosymmetric sublattice at the band-edge.

IV. CONCLUSION

In conclusion, we studied the origin of SHG in a series non-centrosymmetric materials containing lone-pair electrons by analyzing the orbitals on the sublattice. We designed a decision tree to identify the effects of lone-pair electrons on SHG coefficients, and first analyzed the relationship between the interactions and the SHG effect in PbO, PbS and $\beta\text{-SnF}_2$. The study finds that the large SHG effects of these materials are all related to the orbitals of anionic groups. By analyzing the symmetry of the electron structure and calculating the contribution of each interaction orbital to the SHG coefficient in CsPbCO_3F , $\text{PbB}_2\text{O}_3\text{F}_2$ and $\text{PbB}_5\text{O}_7\text{F}_3$, it is shown that strong stereochemically active cation-anion interaction orbitals of lone-pair electrons may contribute more to the SHG. For CsPbCO_3F , the SHG contribution of the Pb 6s orbital is not significant (-2 %). The asymmetry of Pb 6s orbitals in $\text{PbB}_5\text{O}_7\text{F}_3$ and $\text{PbB}_2\text{O}_3\text{F}_2$ contributes more to SHG (6 % and 10 %). To illustrate the role of stereochemically active lead in SHG effects, we substituted barium for lead, which changes the distribution of the band-edge orbitals in $\text{PbB}_5\text{O}_7\text{F}_3$. The phase matching of $\text{BaB}_5\text{O}_7\text{F}_3$ has a significantly blue-shifted (184 nm), and SHG reduced compared to $\text{PbB}_5\text{O}_7\text{F}_3$. The orbitals of the interaction between lead and oxygen are also very significant because these orbitals are located at the band edge and in non-centrosymmetric sublattices.

ACKNOWLEDGMENTS

This work was supported by Key Research Program of Frontier Sciences, Chinese Academy of Sciences (ZDBS-LY-SLH035), the National Natural Science Foundation of China (22193044, 22335007, 52002397 and 22361132544), the National Key R&D Program of China (2021YFB3601502), Natural Science Foundation of Xinjiang (2021D01E05), Tianshan Basic Research Talents (2022TSYCJU0001), and Chinese Academy of Sciences Project for Young Scientists in Basic Research (YSBR-024).

* Electronic address: slpan@ms.xjb.ac.cn

† Electronic address: zhyang@ms.xjb.ac.cn

[1] J. A. Armstrong, N. Bloembergen, J. Ducuing, and P. S.

Pershan, Interactions between light waves in a nonlinear dielectric. *Phys. Rev.* **127**, 1918 (1962).

- [2] Y. R. Shen, Surface properties probed by second-harmonic and sum-frequency generation. *Nature* **337**, 519-525 (1989).
- [3] Y. Ahn, X. Y. Guo, R. Xue, K. J. Qu, K. Sun, D. Mandrus, L. Y. Zhao, *Nat. Photon.* **18**, 26-31 (2024).
- [4] K. Nakagawa, H. Hirori, S. A. Sato, H. Tahara, F. Sekiguchi, G. Yumoto, M. Saruyama, R. Sato, T. Teranishi and Y. Kanemitsu, Size-controlled quantum dots reveal the impact of intraband transitions on high-order harmonic generation in solids. *Nat. Phys.* **18**, 874-878 (2022).
- [5] R. Y. Chen, Y. -H. Luo, J. B. Long, B. Q. Shi, C. Shen and J. Q. Liu, Ultralow-Loss Integrated Photonics Enables Bright, Narrowband, Photon-Pair Sources. *Phys. Rev. Lett.* **133**, 083803 (2024).
- [6] Y. Eliezer, U. Rührmair, N. Wisiol and H. Cao, Tunable nonlinear optical mapping in a multiple-scattering cavity. *PNAS* **120**, e2305027120 (2023).
- [7] L. Kang, and Z. S. Lin, Deep-ultraviolet nonlinear optical crystals: concept development and materials discovery. *Light Sci. Appl.* **11**, 201 (2022).
- [8] T. T. Tran, H. Yu, J. M. Rondinelli, K. R. Poeppelmeier, and P. S. Halasyamani, Deep ultraviolet nonlinear optical materials. *Chem. Mater.* **28**, 5238-5258 (2016).
- [9] C. Wu, X. Jiang, Z. Wang, L. Lin, Z. Huang, X. Long, M. G. Humphrey, Giant optical anisotropy in the UV-transparent 2D nonlinear optical material $\text{Sc}(\text{IO}_3)_2(\text{NO}_3)$. *Angew. Chem. Int. Ed.* **133**, 3506-3510 (2021).
- [10] H. W. Yu, J. Young, H. P. Wu, G. W. Zhang, J. M. Rondinelli, and S. Halasyamani, The next-generation of nonlinear optical materials: $\text{Rb}_3\text{Ba}_3\text{Li}_2\text{Al}_4\text{B}_6\text{O}_{20}\text{F}$ —synthesis, characterization, and crystal growth. *Adv. Opt. Mater.* **5**, 1700840 (2017).
- [11] X. Liu, Y. Yang, M. Li, L. Chen and L. Wu, Anisotropic structure building unit involving diverse chemical bonds: a new opportunity for high-performance second-order NLO materials. *Chem. Soc. Rev.* **52**, 8699-8720 (2023).
- [12] J. P. Foster and F. Weinhold, Natural hybrid orbitals. *J. Am. Chem. Soc.* **102**, 7211-7218 (1980).
- [13] M. Mutailipu, J. Han, Z. Li, F. M. Li, J. J. Li, F. F. Zhang, Z. H. Yang and S. L. Pan, Achieving the full-wavelength phase-matching for efficient nonlinear optical frequency conversion in $\text{C}(\text{NH}_2)_3\text{BF}_4$. *Nat. Photon.* **17**, 694-701 (2023).
- [14] M. S. Dyer, C. Collins, D. Hodgeman, P. A. Chater, A. Demont, S. Romani, R. Sayers, M. F. Michael, B. John and G. R. Darling, Computationally assisted identification of functional inorganic materials. *Science* **340**, 847-852 (2013).
- [15] R. K. Li and C. T. Chen, The theoretical calculation of SHG coefficients of $\beta\text{-BaB}_2\text{O}_4$ crystal. *Acta. Phys. Sin.* **34**, 823-827 (1985).
- [16] A. Walsh, D. J. Payne, R. G. Egdell and G. W. Watton, Stereochemistry of post-transition metal oxides: revision of the classical lone pair model. *Chem. Soc. Rev.* **40**, 4453-4463 (2011).
- [17] S. L. Zhong, X. L. Zhang, S. Liu, S. Y. A. Yang and Y. H. Lu, Giant and nonanalytic negative piezoelectric response in elemental group-Va ferroelectric monolayers. *Phys. Rev. Lett.* **131**, 236801 (2023).
- [18] E. S. Bozin, H. Xie, A. M. M. Abeykoon, S. M. Everett,

- M. G. Tucker, M. G. Kanatzidis and S. J. L. Billinge, Local Sn dipolar-character displacements behind the low thermal conductivity in SnSe thermoelectric. *Phys. Rev. Lett.* **131**, 036101 (2023).
- [19] H. L. Shi, D. Han, S. Y. Chen and M. -H. Du, Impact of metal ns^2 lone pair on luminescence quantum efficiency in low-dimensional halide perovskites. *Phys. Rev. Mater.* **3**, 034604 (2019).
- [20] G. Liu, Y. -Y. Lv, Z. W. Jiang, G. -Z. Liu, X. L. Zhou, Y. Zhang, J. H. Zheng, L. Xu, M. -H. Lu and S. -H. Yao, Mode-selective anharmonicity induced by lone-pair electrons in layered oxyselenides. *Phys. Rev. B* **109**, 024302 (2024).
- [21] P. S. Halasyamani and J. M. Rondinelli, The must-have and nice-to-have experimental and computational requirements for functional frequency doubling deep-UV crystals. *Nat. Commun.* **9**, 2972 (2018).
- [22] S. H. Yang, H. Xue and S. P. Guo, Borates as promising electrode materials for rechargeable batteries. *Coord. Chem. Rev.* **427**, 213551 (2021).
- [23] Y. Y. Yang, Y. Xiao, B. X. Li, Y. -G. Chen, P. H. Guo, B. B. Zhang, X. -M. Zhang, Stereochemically active lone-pair containing metal substitution in polar axis toward a giant phase-matchable optical nonlinear silicate crystal $\text{Li}_3(\text{OH})\text{PbSiO}_4$. *J. Am. Chem. Soc.* **145**, 22577-22583 (2023).
- [24] J. Chen, C. L. Hu, F. Kong and J. M. Mao, High-performance second-harmonic-generation (SHG) materials: new developments and new strategies. *Acc. Chem. Res.* **54**, 2775-2783 (2021).
- [25] C. T. Chen, An ionic grouping theory of the electro-optical and non-linear optical effects of crystals (II)—a theoretical calculation of the second harmonic optical coefficients of the lithium iodate crystal based on a highly deformed oxygen-octahedra model (I). *Acta. Phys. Sin.* **26**, 124-132 (1977).
- [26] A. Rosenzweig and B. Morosin, A reinvestigation of the crystal structure of LiIO_3 . *Acta. Crystallogr.* **20**, 758 (1966).
- [27] Y. C. Liu, X. M. Liu, S. Liu, Q. R. Ding, Y. Q. Li, L. N. Li, S. G. Zhao, Z. S. Lin, J. H. Luo and M. C. Hong, An unprecedented antimony(III) borate with strong linear and nonlinear optical responses. *Angew. Chem. Int. Ed.* **59**, 7793-7796 (2020).
- [28] G. H. Zhou, L. Huang, N. Ye, C. S. Lin, W. D. Cheng, H. Huang, CsPbCO_3F : a strong second-harmonic generation material derived from enhancement via $p-\pi$ interaction. *J. Am. Chem. Soc.* **135**, 18560-18566 (2013).
- [29] van de Walle. A, A complete representation of structure-property relationships in crystals. *Nat. Mater.* **7**, 455-458 (2008).
- [30] G. Kresse and J. Furthmüller, Efficient iterative schemes for *ab initio* total-energy calculations using a plane-wave basis set. *Phys. Rev. B* **54**, 11169 (1996).
- [31] J. P. Perdew, K. Burke and M. Ernzerhof, generalized gradient approximation made simple. *Phys. Rev. Lett.* **78**, 3865-3868 (1996).
- [32] J. Heyd, G. E. Scuseria and M. Ernzerhof, Hybrid functionals based on a screened Coulomb potential. *J. Chem. Phys.* **118**, 8207-8215 (2003).
- [33] A. V. Krukau, O. A. Vydrov, A. F. Izmaylov and G. E. Scuseria, Influence of the exchange screening parameter on the performance of screened hybrid functionals. *J. Chem. Phys.* **125**, 224106 (2006).
- [34] G. Pizzi, V. Vitale, R. Arita, S. Blügel, F. Freimuth, G. Géranton, M. Gibertini, D. Gresch, C. Johnson, T. Koretsune, J. Ibañez-Azpiroz, H. Lee, J.-M. Lihm, D. Marchand, A. Marrazzo, Y. Mokrousov, J. I. Mustafa, Y. Nohara, Y. Nomura and L. Paulatto, Wannier90 as a community code: new features and applications. *J. Phys.: Condens. Matter.* **32**, 165902 (2020).
- [35] N. Marzari, A. A. Mostofi, J. R. Yates, I. Souza and D. Vanderbilt, Maximally localized Wannier functions: Theory and applications. *Rev. Mod. Phys.* **84**, 1419 (2012).
- [36] C. Aversa and J. E. Sipe, Nonlinear optical susceptibilities of semiconductors: Results with a length-gauge analysis. *Phys. Rev. B* **52**, 14636-14645 (1995).
- [37] S. N. Rashkeev, W. R. L. Lambrecht, B. Segall, Efficient *ab initio* method for the calculation of frequency-dependent second-order optical response in semiconductors. *Phys. Rev. B* **57**, 3905-3919 (1998).
- [38] J. Lin, M. -H. Lee, Z. -P. Liu, C. T. Chen, C. J. Pickard, Mechanism for linear and nonlinear optical effects in $\beta\text{-BaB}_2\text{O}_4$ crystals. *Phys. Rev. B* **60**, 13380 (1999).
- [39] B. -H. Lei, S. L. Pan, Z. H. Yang, C. Cao and D. J. Singh, Second harmonic generation susceptibilities from symmetry adapted Wannier functions. *Phys. Rev. Lett.* **125**, 187402 (2020).
- [40] F. M. Li, W. Q. Jin, R. An, M. Mutaupipu, S. L. Pan and Z. H. Yang, Covalently bonded fluorine optimizing deep-ultraviolet nonlinear optical performance of fluorooxoborates. *Sci. Bull.* **69**, 1192-1196 (2024).
- [41] T. Lu and F. W. Chen, Multiwfn: A multifunctional wavefunction analyzer. *J. Comput. Chem.* **33**, 580-592 (2012).